



 Cite this: *RSC Adv.*, 2021, 11, 38589

Highly enhanced electrical properties of lanthanum-silicate-oxide-based SOFC electrolytes with co-doped tin and bismuth in $\text{La}_{9.33-x}\text{Bi}_x\text{Si}_{6-y}\text{Sn}_y\text{O}_{26}$

 Atiek Rostika Noviyanti, ^{*a} Juliandri,^a Suci Winarsih,^b Dani Gustaman Syarif,^c Yoga Trianzar Malik,^a Rifki Septawendar^d and Risdiana^b

Solid oxide fuel cells (SOFCs) are one of the most promising clean energy sources to be developed. However, the operating temperature of SOFCs is currently still very high, ranging between 1073 and 1273 K. Reducing the operating temperature of SOFCs to intermediate temperatures in between 773 and 1073 K without decreasing the conductivity value is a challenging research topic and has received much attention from researchers. The electrolyte is one of the components in SOFCs which has an important role in reducing the operating temperature of the SOFC compared to the other two fuel cell components, namely the anode and cathode. Therefore, an electrolyte that has high conductivity at moderate operating temperature is needed to obtain SOFC with medium operating temperature as well. $\text{La}_{9.33}\text{Si}_6\text{O}_{26}$ (LSO) is a potential electrolyte that has high conductivity at moderate operating temperatures when this material is modified by doping with metal ions. Here, we report a modification of the structure of the LSO by partial substitution of La with Bi^{3+} ions and Si with Sn^{4+} , which forms $\text{La}_{9.33-x}\text{Bi}_x\text{Si}_{6-y}\text{Sn}_y\text{O}_{26}$ with $x = 0.5, 1.0, 1.5$, and $y = 0.1, 0.3, 0.5$, in order to obtain an electrolyte of LSO with high conductivity at moderate operating temperatures. The addition of Bi and Sn as dopants has increased the conductivity of the LSO. Our work indicated highly enhanced electrical properties of $\text{La}_{7.83}\text{Bi}_{1.5}\text{Si}_{5.7}\text{Sn}_{0.3}\text{O}_{26}$ at 873 K ($1.84 \times 10^{-2} \text{ S cm}^{-1}$) with considerably low activation energy (E_a) of 0.80 eV comparing to pristine $\text{La}_{9.33}\text{Si}_6\text{O}_{26}$ ($0.08 \times 10^{-2} \text{ S cm}^{-1}$).

Received 28th September 2021

Accepted 18th November 2021

DOI: 10.1039/d1ra07223d

rsc.li/rsc-advances

Introduction

Solid oxide fuel cells (SOFCs) are energy devices that convert chemical reactions into electricity and produce up to 10 MW of electrical power. An SOFC has three main components: a cathode that reduces fuel, a solid electrolyte responsible for delivering oxygen ions, and an anode that reduces oxygen gas to become oxygen ions.

General SOFCs typically operate at high temperatures in the range between 1073 K and 1273 K,¹ which causes accelerated aging and damaging their components. Therefore, lowering the operating temperature is an important issue that must be developed in SOFC. In addition, lowering its working temperature is also

necessary to eliminate power loss during operation. However, a decrease in operating temperature usually causes a decrease in SOFC performance. To resolve these problems, the use of high conductivity electrolytes is a very determining factor and must be considered when manufacturing SOFC. High conductivity electrolytes are usually obtained from new types of electrolytes, or modifications to existing electrolytes. However, finding new types of electrolytes is more difficult than modifying existing electrolytes. The usual modification by defect formation in crystals can be done by doping and forming composite. Electrolyte modification usually also correlates with other improvements in physical properties such as reduced brittleness and obtained high-density electrolytes with lower sintering temperature. The electrolyte from apatite type is an alternative electrolyte to overcome this problem² because of the large conduction tunnel in apatite lattice structure, facilitating the circulation of free oxide ions³ which allows the increased conductivity of the electrolyte. LSO with a hexagonal crystal structure with three possible space clusters namely $P\bar{3}$, $P6_3$ and $P6_3/m$ was first discovered by Nakayama *et al.*⁴ The electrolytes of the LSO generally exhibit insufficient conductivity at lower operating temperatures below 973 K. However, the open structure of the LSO allows modification by the doping technique on the La

^aDepartment of Chemistry, Faculty of Mathematics and Natural Sciences, Universitas Padjadjaran, Jl. Raya Bandung-Sumedang km 21 Jatinangor, Sumedang, West Jawa 45363, Indonesia. E-mail: atiek.noviyanti@unpad.ac.id

^bDepartment of Physics, Faculty of Mathematics and Natural Sciences, Universitas Padjadjaran, Jl. Raya Bandung-Sumedang km 21 Jatinangor, Sumedang, West Jawa 45363, Indonesia

^cPRINT-ORTN-BRIN, Jl. Taman Sari 71, Bandung 40132, Indonesia

^dLaboratory of Advanced Ceramics, Glass, and Enamel, Center for Ceramics, Ministry of Industry of Indonesia, Indonesia



and Si site which makes it possible to obtain sufficient conductivity values at low-temperature operation.⁵ Several studies reported that by adding dopants to the apatite lattice structures at the La and Si sites, the conductivity can be increased.^{5,6} Some of the dopants that have been reported to substitute La and Si in LSO are Sr,^{7,9} Ca,⁷ Ba,^{2,10} Mg,¹¹ Cu,¹² Co,¹³ W,¹⁰ and Ti.¹⁴ Noviyanti *et al.*¹⁵ added 0.5 and 1.0 of Bi dopant at the La site, while Xiang *et al.*¹⁶ reported that 0.5 doping of Sn at the Si site resulted in conductivity values of 2.46×10^{-4} S cm⁻¹ at 773 K and 5.71×10^{-3} S cm⁻¹ at 1073 K. Whereas various Bi doping at composition of $0.5 \leq x \leq 2$ on La_{10-x}Bi_x(SiO₄)₆O₃ resulted in a conductivity of 2.4×10^{-4} S cm⁻¹ at 973 K,¹⁷ Abbassi *et al.*¹⁸ also reported that doping of Bi in CaBaLa₆Bi₂(SiO₄)₆O₂ has resulted a conductivity of 2.20×10^{-5} S cm⁻¹ at 873 K. However, the simultaneous use of Bi and Sn doping at La and Si sites in the LSO-apatite structure has not been reported before. Therefore, this study aims to study the effect of various concentrations of Bi- and Sn-dopant substituted at La and Si sites on the La_{9.33-x}Si_{6-y}O₂₆ structure. To be utilized as an electrolyte of SOFC, the LSO must be synthesized into a solid membrane which is prepared by sintering at high temperatures. It should also be noted that to obtain a high quality and solid membrane, the sintering temperatures of LSO require high temperatures of up to 1873 K.^{22,23,25,26} Therefore, the use of dopants that have the dual advantages of increasing conductivity and lowering the sintering temperature is an important step to obtain high-quality membranes. Bi is known to have the ability to increase conductivity¹⁷⁻¹⁹ as well as reduce sintering temperature.^{19,24} Meanwhile, Sn is known to be suitable support on Si site which can improve the total conductivity.²⁶ The hydrothermal method was chosen as the synthesis method, in order to obtain a good crystalline powder and high purity.⁶ Here, we reported a study of the structure and electrical properties of La_{9.33-x}Bi_xSi_{6-y}Sn_yO₂₆, in which the Bi³⁺ and Sn⁴⁺ were used simultaneously as doping at La and Si sites in various concentration. Our study offers the co-doping strategy of Sn and Bi to enhance the electrical properties several times higher than the pristine LSO and previously reported value.

Experimental procedure

The materials of La_{9.33-x}Bi_xSi_{6-y}Sn_yO₂₆-apatite type with $x = 0.5, 1.0, 1.5$ and $y = 0.1, 0.3, 0.5$ were prepared from high-purity La₂O₃ (Sigma Aldrich, 99.999%), Na₂SiO₃·5H₂O (Sigma Aldrich, 97%), Bi₂O₃, Sn₂O₃, and NaOH (Merck, 99%).

The experimental design in the synthesis of La_{9.33-x}Bi_xSi_{6-y}Sn_yO₂₆-apatite type with $x = 0.5, 1.0, 1.5$ and $y = 0.1, 0.3, 0.5$ are listed in Table 1.

Lanthanum oxide was initially calcined for the decarbonation purpose at 1373 K for 10 hours. Then, a certain amount of Na₂SiO₃ was weighed and dissolved in a 50 mL of a 3 M NaOH solution. A solution of Na₂SiO₃ was mixed with La₂O₃, SnO₂, and Bi₂O₃. The mixture was transferred into the autoclave and heated in an oven at 503 K for 3 days. The resulting product was washed with deionized water, then filtered and dried in an oven at 393 K for 24 hours.² All samples were pelleted then sintered at 1773 K for 8 hours.

The structures of the La_{9.33-x}Bi_xSi_{6-y}Sn_yO₂₆ were determined using a Phillips Analytical X-ray PW3373 diffractometer with a CuK_α radiation source ($\lambda = 0.15$ nm). The diffraction patterns were scanned from 10 to 80°. The crystal lattice parameters and its cell unit volume were analysed by using a General Structure and Analysis Software II (GSAS-II) and refined by using a pattern from JCPDS no. 04-011-7781 and no. 00-049-0443, for La_{9.33-x}Si_{6-y}O₂₆ (LSO) and La_{9.33-x}Bi_xSi_{6-y}Sn_yO₂₆, respectively.

The effect of the Bi³⁺ and Sn⁴⁺ dopant concentrations in the apatite conductivity was tested using Electrochemical Impedance Spectroscopic (EIS, GW Instek 6105G LCR meter). The sintered pellets were coated with silver paste on both sides with the effective area (*A*) of 0.026 cm⁻², and then heated at 873 K for 10 minutes. The pellets are connected with platinum wire to the electrodes where the silver paste is coated. Impedance spectroscopic measurements were carried out at the range between 20 Hz and 5 MHz, a voltage of 1 V and at a range temperature of 573–1073 K. Based on the EIS measurement, the obtained Nyquist plots were interpreted using EIS analyzer. The conductivity value is calculated using the eqn (1).

$$\sigma = L \frac{R}{A} \quad (1)$$

where σ = conductivity, L = thickness of pellets (cm), R = resistance (ohms) and A = area of effective electrode (cm).

Result and discussion

Structure

La_{9.33-x}Bi_xSi_{6-y}Sn_yO₂₆-apatite type electrolytes were successfully synthesized *via* a hydrothermal method. Fig. 1 depicts

Table 1 The precursors and the target compounds of La_{9.33-x}Bi_xSi_{6-y}Sn_yO₂₆

Target compounds	Sample code	Weight (g)			
		Precursors		Dopants	
		La ₂ O ₃	Na ₂ SiO ₃ ·5H ₂ O	Bi ₂ O ₃	SnO ₂
La _{9.33} Si ₆ O ₂₆	I	1.6165	1.3534	—	—
La _{8.83} Bi _{0.5} Si _{5.9} Sn _{0.1} O ₂₆	II	1.4948	1.3003	0.1211	0.0157
La _{8.83} Bi _{0.5} Si _{5.7} Sn _{0.3} O ₂₆	III	1.4809	1.2445	0.1199	0.0465
La _{8.83} Bi _{0.5} Si _{5.5} Sn _{0.5} O ₂₆	IV	1.4672	1.1892	0.1188	0.0769
La _{8.33} Bi ₁ Si _{5.7} Sn _{0.3} O ₂₆	V	1.3723	1.2225	0.2356	0.0457
La _{7.83} Bi _{1.5} Si _{5.7} Sn _{0.3} O ₂₆	VI	1.2674	1.2012	0.3472	0.0449



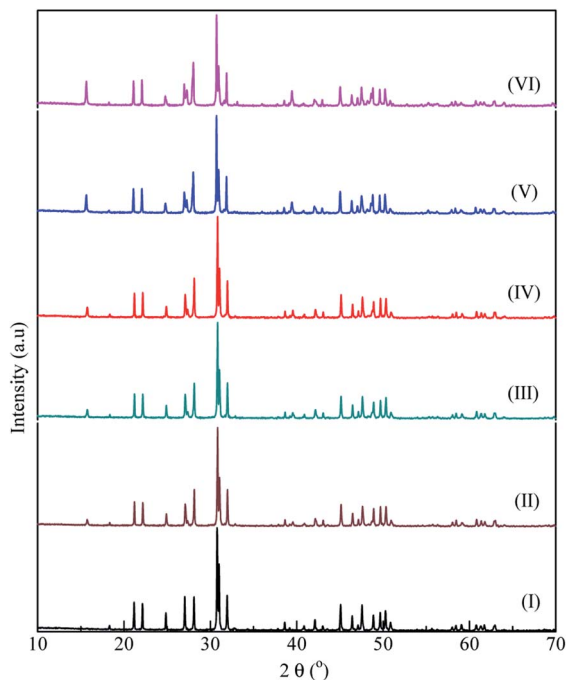


Fig. 1 The XRD patterns of co-doped $\text{La}_{9.33-x}\text{Bi}_x\text{Si}_{6-y}\text{Sn}_y\text{O}_{26}$ apatite phases in various value of x and y for samples with code I–VI.

Table 2 Lattice constants and volume of unit cell of LSO and co-doped LSO-based materials

Sample	Sample code	$a = b$ (Å)	c (Å)	Cell unit volume (Å ³)
$\text{La}_{9.33}\text{Si}_6\text{O}_{26}$	I	9.695	7.179	584.413
$\text{La}_{8.83}\text{Bi}_{0.5}\text{Si}_{5.9}\text{Sn}_{0.1}\text{O}_{26}$	II	9.702	7.178	585.120
$\text{La}_{8.83}\text{Bi}_{0.5}\text{Si}_{5.7}\text{Sn}_{0.3}\text{O}_{26}$	III	9.705	7.178	585.571
$\text{La}_{8.83}\text{Bi}_{0.5}\text{Si}_{5.5}\text{Sn}_{0.5}\text{O}_{26}$	IV	9.702	7.178	585.209
$\text{La}_{8.33}\text{Bi}_1\text{Si}_{5.7}\text{Sn}_{0.3}\text{O}_{26}$	V	9.724	7.183	588.276
$\text{La}_{7.83}\text{Bi}_{1.5}\text{Si}_{5.7}\text{Sn}_{0.3}\text{O}_{26}$	VI	9.720	7.183	587.844

a XRD pattern of $\text{La}_{9.33-x}\text{Bi}_x\text{Si}_{6-y}\text{Sn}_y\text{O}_{26}$ -apatite type structure with various value of x and y . For comparison, the XRD pattern of LSO samples was also displayed. It is found that all main peaks of LSO are observed in all samples.

The main peaks of LSO are observed at diffraction angles, 2θ , of 21.1° , 22° , 24.8° , 27° , 28° , 30.7° , 30.9° , 31.9° , 32.7° , 38.5° , 39° ,

40.7° , 42° , 42.9° , 45° , 46.3° , 47.4° , 48.8° , 49.6° in accordance with the structure of $\text{La}_{9.33}\text{Si}_6\text{O}_{26}$.^{2,4} The secondary phase consistently appeared in all the co-doped LSO-apatite at around diffraction angle of $15\text{--}15.5^\circ$ with various intensities as shown in Fig. 1. The intensity of the peak at the 2θ of 15° elevated with the increasing content of the Bi-doping. Adding a higher of Bi-doping in the La site of LSO should be eliminating the phase impurities at this 2θ region.¹⁵ However, we found contrastly in this study at which the higher content of Bi with the co-existence of Sn-doping in $\text{La}_{9.33-x}\text{Bi}_x\text{Si}_{6-y}\text{Sn}_y\text{O}_{26}$ may possibly lead to the disintegration of the La ions, resulting in $\text{La}(\text{OH})_3$ phase.

The Rietveld refinement's result shows that the entire apatite-type electrolyte has hexagonal-based crystal structure with $P\bar{3}$ space group. The certain amount of dopant may change the lattice parameter as shown in Table 2. A larger dopant of Bi^{3+} , with the radius of 1.17 Å, prefers the La site (La^{3+} radius = 1.15 Å). Meanwhile, a smaller dopant such as Sn^{4+} that exhibits the radius of 0.71 Å prefers the Si site (Si^{4+} radius = 0.41 Å).^{8,16} The greater the Bi concentration, the higher the lattice parameter both on the a - and c -axis. It is because the size of Bi is larger than that of La, especially seen in samples V and VI with Bi concentrations of 1 and 1.5 respectively, as listed in Table 1 and Fig. 2. The possible reasons for increasing the lattice parameters and volume of the unit cell first and then decreasing gradually are as follow: first, the existence of impurity that disturbing the position of atoms or decreasing the content of several atoms in the crystals structure, second, the simultaneous doping of two atoms causes opposite effects to each other in certain compositions.

The simulations of the positions of La, Si, and O atoms in the LSO structure are shown in Fig. 3. Based on their positions, La, Si, and O atoms are divided into La1, La2, La3, Si, O1, O2, O3, O4, O5, and O6. It is well known that O6 is interstitial oxygen due to a Frenkel defect that is formed due to the influence of Bi and Sn doping.²⁰ The atomic coordinates for all atoms including the site occupation factor are listed in Table 3.

The bond lengths between the atoms at the LSO for all samples are summarized in Table 4. Changes in bond length of all La–O bonds and Si–O bonds due to the doping effect of Bi and Sn are clearly observed in sample V and sample VI. These changes can also result in the enlargements of the unit cell and create structural imbalances that can affect their physical properties as expected.

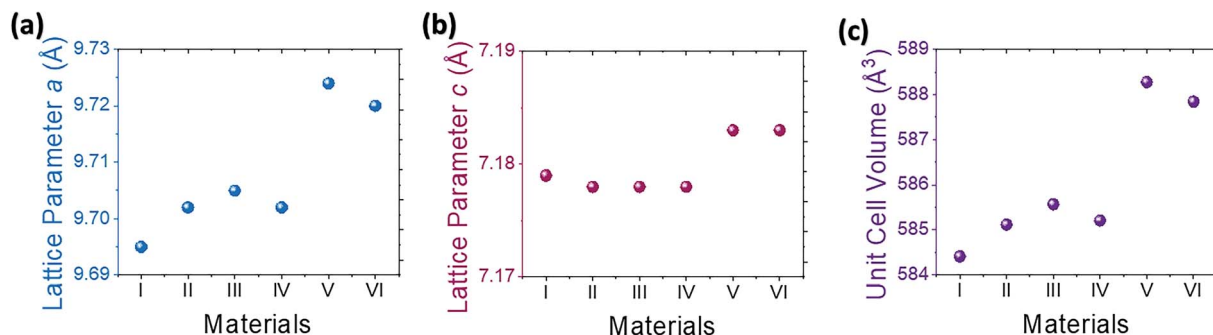


Fig. 2 Refined structural parameter of each sample (a) lattice constant a (b) lattice constant c (c) unit cell volume.



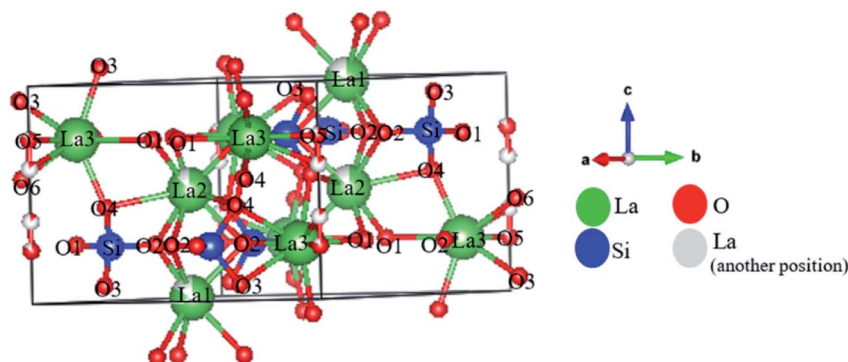


Fig. 3 Atomic coordinate of LSO-apatite-type structure.

Table 3 Atomic coordinate of $\text{La}_{9.33}\text{Si}_6\text{O}_{26}$

Atom	Site	x	y	z	Site occupation factor
La1	2d	1/3	2/3	-0.0086(7)	0.83(2)
La2	2d	1/3	2/3	0.4948(6)	0.86(2)
La3	6g	0.0138(2)	0.2445(1)	0.2527(8)	0.98(1)
Si	6g	0.4005(3)	0.3709(2)	0.25	1.0
O1	6g	0.3223(2)	0.4829(2)	0.2572(9)	1.0
O2	6g	0.5942(2)	0.4722(2)	0.2522(9)	1.0
O3	6g	0.3377(7)	0.2518(7)	0.0731(7)	1.0
O4	6g	0.3491(6)	0.2569(7)	0.4329(7)	1.0
O5	2c	0.0	0.0	0.245(3)	0.84(2)
O6	2c	0.0	0.0	0.379(6)	0.14(1)

Conductivity

All samples were designed with the same void concentration (La = 9.33) and oxygen content (O = 26) so that changes in conductivity could be directly compared and evaluated as the effect of Bi and Sn doping concentrations on doped-LSO. The conductivity of the LSO and doped-LSO is shown in Fig. 4 and

Table 4 Bond distance of LSO and co-doped LSO-based materials

Bond distance (Å)	Sample code					
	I	II	III	IV	V	VI
La1-O1	2.576	2.577	2.577	2.577	2.581	2.580
La1-O2	2.512	2.512	2.513	2.513	2.516	2.516
La1-O3	2.914	2.915	2.916	2.916	2.922	2.922
La2-O1	2.430	2.430	2.431	2.431	2.435	2.434
La2-O2	2.559	2.560	2.561	2.560	2.564	2.564
La2-O3	2.497	2.499	2.500	2.499	2.505	2.504
La3-O1	2.716	2.718	2.718	2.718	2.724	2.723
La3-O2	2.497	2.499	2.500	2.500	2.505	2.504
La3-O3	2.588	2.589	2.590	2.589	2.594	2.594
La3-O4	2.435	2.435	2.435	2.430	2.437	2.437
La3-O5	2.307	2.309	2.310	2.309	2.314	2.313
La3-O6	2.478	2.480	2.480	2.480	2.485	2.484
Si-O1	1.606	1.607	1.608	1.607	1.611	1.610
Si-O2	1.627	1.628	1.629	1.628	1.632	1.631
Si-O3	1.617	1.617	1.617	1.617	1.619	1.619
Si-O4	1.626	1.626	1.626	1.626	1.628	1.628

Table 5. It is found that the doping effect of Bi and Sn appears to significantly affect their conductivity. The Nyquist plot showed decreasing a semi-circle impedance as varied Sn dopants which suggested an increasing of the conductivities. For example, the conductivity of sample V, which $\sigma_{873\text{ K}}$ of $1.37 \times 10^{-2} \text{ S cm}^{-1}$, increased almost twice comparing to sample III ($\sigma_{873\text{ K}} = 0.74 \times 10^{-2} \text{ S cm}^{-1}$). Bi and Sn doping also have the effect of reducing the E_a from 0.69 to 0.76 eV, which indicates that the movement of oxide ions is facilitated in the doped-apatite structure. In addition, the doping concentration also significantly affects the increase in conductivity. Increasing the Sn concentration from 5% ($y = 0.3$) to $\sim 8.3\%$ ($y = 0.5$) as in sample IV actually decreased its conductivity. However, on the other hand, a different effect is shown by Bi doping. It was found that increasing the Bi concentration tended to increase its conductivity as well, as shown in samples V and VI. It is found that sample VI of $\text{La}_{7.83}\text{Bi}_{1.5}\text{Si}_{5.7}\text{Sn}_{0.3}\text{O}_{26}$ has the highest value of conductivity of $1.84 \times 10^{-2} \text{ S cm}^{-1}$ at 873 K.

The significant increase in conductivity values in samples V and VI can be explained by changes in the bond length between La-O and Si-O. High conductivity is found in doped-LSO which have the longest La-O and Si-O bond lengths. The addition of the La-O and Si-O bond lengths caused the channel on the c -axis to expand as well, thereby facilitating the movement of oxide ions. Especially for the effect of adding Sn-dopant to the Si site in samples I to IV, the conductivity value increased with increasing Sn from 0 to 0.3 (sample I to sample III). However, a bit increasing of Sn dopant (0.5) dropped the conductivity almost twice from 0.74 to 0.38 S cm^{-1} . The maximum conductivity value was obtained when Sn was 0.3 (sample III). The reason for this data may be explained by looking at the conduction pathway at the position of La at site 6g. An increase in Sn at the Si site in excess of 0.3 can inhibit the ionic conduction pathway by disrupting the position of La at site 6 and pushing it into a narrow conduction pathway, which results in a low conductivity value as produced by sample IV.

The E_a lower than 1.1 eV indicates the ion conduction pathways at which adopting an interstitial ion migration mechanism at the temperature range of 573 to 873 K.²¹ The existence of the O6 site obtained a from the simulation results confirmed that the dominant mechanism in the conduction of



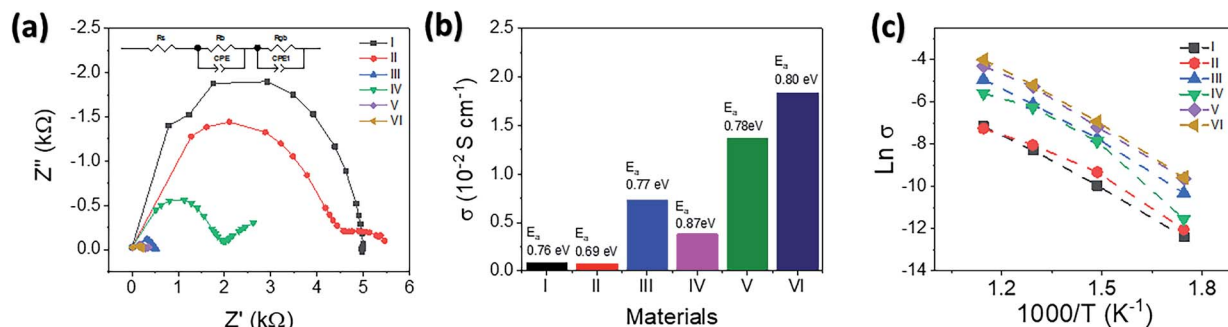


Fig. 4 Electrical properties of LSO and co-doped LSO. Nyquist impedance (a) and conductivity (b) at 873 K, and (c) Arrhenius plot from conductivity at different measurement temperatures (573, 673, 773 and, 873 K).

Table 5 The value of conductivity at 873 K and E_a of $\text{La}_{9.33-x}\text{Bi}_x\text{Si}_{6-y}\text{Sn}_y\text{O}_{26}$

Composition	Sample code	Conductivity (σ)/ $\times 10^{-2}$ S cm^{-1}	Linear regression from Arrhenius plot	Activation energy (E_a)/eV
$\text{La}_{9.33}\text{Si}_6\text{O}_{26}$	I	0.08	$\text{Ln } \sigma = -8.77 (1000/T) + 2.98; R^2 = 0.998$	0.76
$\text{La}_{8.83}\text{Bi}_{0.5}\text{Si}_{5.9}\text{Sn}_{0.1}\text{O}_{26}$	II	0.07	$\text{Ln } \sigma = -7.99 (1000/T) + 2.18; R^2 = 0.997$	0.69
$\text{La}_{8.83}\text{Bi}_{0.5}\text{Si}_{5.7}\text{Sn}_{0.3}\text{O}_{26}$	III	0.74	$\text{Ln } \sigma = -8.99 (1000/T) + 5.48; R^2 = 0.997$	0.77
$\text{La}_{8.83}\text{Bi}_{0.5}\text{Si}_{5.5}\text{Sn}_{0.5}\text{O}_{26}$	IV	0.38	$\text{Ln } \sigma = -10.07 (1000/T) + 6.46; R^2 = 0.956$	0.87
$\text{La}_{8.33}\text{Bi}_{1.0}\text{Si}_{5.7}\text{Sn}_{0.3}\text{O}_{26}$	V	1.37	$\text{Ln } \sigma = -9.06 (1000/T) + 6.25; R^2 = 0.996$	0.78
$\text{La}_{7.83}\text{Bi}_{1.5}\text{Si}_{5.7}\text{Sn}_{0.3}\text{O}_{26}$	VI	1.84	$\text{Ln } \sigma = -9.33 (1000/T) + 6.81; R^2 = 0.997$	0.80

LSO and doped-LSO is the insertion mechanism. The E_a value of each sample together with the value of conductivity is presented in Table 5. Generally, the E_a is lowered after an introduction of Bi dopant with constant Sn concentration. A bit enhancement of Sn dopant to the system drastically declines the σ along with increase the E_a . With the same Bi content ($x = 0.5$), E_a elevated from 0.69 to 0.87 eV as increasing Sn dopant (from 0.1 to 0.5) which also showed the similar behaviour with the same Sn concentration of 0.3 and increasing of Bi dopant from 0.5 to 1.5 with E_a increased from 0.77 to 0.80 eV.

Conclusions

The materials of co-doping of Bi and Sn in the structure of $\text{La}_{9.33-x}\text{Bi}_x\text{Si}_{6-y}\text{Sn}_y\text{O}_{26}$ -apatite with $x = 0.5, 1, \text{ and } 1.5$ and $y = 0.1, 0.3, \text{ and } 0.5$ were successfully synthesized by using a hydrothermal method. All main peaks of LSO are observed in all samples. The conductivity of the $\text{La}_{9.33-x}\text{Bi}_x\text{Si}_{6-y}\text{Sn}_y\text{O}_{26}$ -apatite type increased as the Bi-doping content increases. $\text{La}_{7.83}\text{Bi}_{1.5}\text{Si}_{5.7}\text{Sn}_{0.3}\text{O}_{26}$ has the highest value of conductivity as 1.84×10^{-2} S cm^{-1} at 873 K with the activation energy (E_a) value of 0.80 eV which indicates the adoption of the interstitial ionic conduction migration pathways. Our study can open a new possibility of structure modification of lanthanum-oxide-based SOFC electrolyte to achieve high electrochemical performance for the application in the clean energy generation.

Author contributions

A. R. N.-conceptualisation, writing-original draft, writing-revision, investigation; J. J.-supervision, formal analysis; S. W.-data curation; R. R.-writing-revision, supervision, formal analysis; D. G. S.-resources; Y. T. M.-writing-revision, formal analysis, investigation, data curation; R. S.-writing-revision.

Conflicts of interest

There are no conflicts to declare.

Acknowledgements

Authors would like to thank Ministry of Research and Technology, Republic of Indonesia through PDUPT Research grant No. 1207/UN6.3.1/PT.00/2021 for funding this research. This work also partially supported by Academic Leadership Grant of Universitas Padjadjaran 2021 no. 1959/UN6.3.1/PT.00/2021. SW also would like to thank Universitas Padjadjaran for the Post-Doctoral Research grant no. 3570/UN6.3.3/LT/2020. We also gratefully say to Shofia Utari Agustina for preparing sample.

References

- 1 Y. Wu, *et al.*, Enhanced redox-stable $\text{Sm}_{0.5}\text{Sr}_{0.5}\text{FeO}_{3-\delta}$ electrode material for symmetric solid oxide fuel cells at reduced temperatures, *Ceram. Int.*, 2020, **46**(5), 6714–6722, DOI: 10.1016/j.ceramint.2019.11.160.



- 2 A. Noviyanti, B. Prijamboedi, N. Marsih and I. Ismunandar, Hydrothermal preparation of apatite-type phases $\text{La}_{9.33}\text{Si}_6\text{O}_{26}$ and $\text{La}_9\text{M}_1\text{Si}_6\text{O}_{26.5}$ (M = Ca, Sr, Ba), *ITB J. Sci.*, 2012, **44A**(2), 193–203, DOI: 10.5614/itbj.sci.2012.44.2.8.
- 3 M. A. Melkozerova, *et al.*, Intrinsic defects and their influence on optical properties of $\text{ALa}_9(\text{GeO}_4)_6\text{O}_2$ (A = Li, Na, K, Rb, Cs) oxyapatites prepared by spray pyrolysis, *J. Alloys Compd.*, 2020, **839**, 155609, DOI: 10.1016/j.jallcom.2020.155609.
- 4 S. Nakayama, T. Kageyama, H. Aono and Y. Sadaoka, Ionic Conductivity of Lanthanoid Silicates, $\text{Ln}_{10}(\text{SiO}_4)_6\text{O}_3$ (Ln = La, Nd, Sm, Gd, Dy, Y, Ho, Er and Yb), *J. Mater. Chem.*, 1995, **11**(11), 1801–1805.
- 5 C. Wu, *et al.*, Improving conductivity of apatite-type lanthanum silicate by Nd and Zn co-doping, *J. Alloys Compd.*, 2020, **827**, 154331, DOI: 10.1016/j.jallcom.2020.154331.
- 6 A. R. Noviyanti, D. R. Eddy and A. Anshari, Synthesis of the Bi-doped apatite-type phases $\text{La}_{10-x}\text{Bi}_x\text{Si}_6\text{O}_{27}$ (x = 0.5, and 1) by hydrothermal method, *Procedia Chem.*, 2015, **17**, 16–20, accessed: Aug. 20, 2018. [Online]. Available: <https://www.sciencedirect.com/science/article/pii/S1876619615002594>.
- 7 C. Wu, Z. Huang, C. Chen, H. Lei, S. Chen and Y. Jiang, Preparation of zinc and alkaline earth metal co-doped apatite-type lanthanum silicate electrolyte ceramics by combustion method and mechanism of co-doping enhanced conductivity, *Ceram. Int.*, 2020, **46**(15), 24661–24667, DOI: 10.1016/j.ceramint.2020.06.255.
- 8 A. R. Noviyanti, D. R. Eddy, H. Iwan, D. Muhammad and S. D. Gustaman, Sn (IV) doped lanthanum silicate apatite structure ($\text{La}_{9.33}\text{Si}_{6-x}\text{Sn}_x\text{O}_{26}$; x: 0.1; 0.3; 0.5) as an electrolyte, *Res. J. Chem. Environ.*, 2018, **22**(special issue August), 337–341.
- 9 X. G. Cao and S. P. Jiang, Effect of Sr and Al or Fe co-doping on the sinterability and conductivity of lanthanum silicate oxyapatite electrolytes for solid oxide fuel cells, *Int. J. Hydrogen Energy*, 2014, **39**(33), 19093–19101, DOI: 10.1016/j.ijhydene.2014.09.092.
- 10 Y. Zhao, L. Dai, Z. He, L. Wang and J. Cao, Synthesis and characterization of Ba^{2+} and W^{6+} co-doped apatite-type lanthanum silicate electrolytes, *Ceram. Int.*, 2020, **46**(4), 5420–5429, DOI: 10.1016/j.ceramint.2019.10.299.
- 11 C. Timurkutluk, B. Timurkutluk and Y. Kaplan, Experimental optimization of the fabrication parameters for anode-supported micro-tubular solid oxide fuel cells, *Int. J. Hydrogen Energy*, 2020, **45**(43), 23294–23309, DOI: 10.1016/j.ijhydene.2020.06.060.
- 12 T. Yang, H. Zhao, M. Fang, K. Świerczek, J. Wang and Z. Du, A new family of Cu-doped lanthanum silicate apatites as electrolyte materials for SOFCs: synthesis, structural and electrical properties, *J. Eur. Ceram. Soc.*, 2019, **39**(2), 424–431, DOI: 10.1016/j.jeurceramsoc.2018.08.047.
- 13 Q. Shi, L. Lu, H. Jin, H. Zhang and Y. Zeng, Electrical properties and thermal expansion of cobalt doped apatite-type lanthanum silicates based electrolytes for IT-SOFC, *Mater. Res. Bull.*, 2012, **47**(3), 719–723, DOI: 10.1016/j.materresbull.2011.12.015.
- 14 A. R. Noviyanti, *et al.*, Synthesis and conductivities of the Ti-doped apatite-type phases $\text{La}_{9.33}\text{Si}_{6-x}\text{Ti}_x\text{O}_{26}$, *J. Phys.: Conf. Ser.*, 2018, **1080**, 012018.
- 15 A. R. Noviyanti, N. Akbar, I. Hastiawan, I. Rahayu, H. Haryono, Y. T. Malik and R. Risdiana, Bi doping effect on the conductivity of lanthanum silicate apatite, *Mater. Sci. Forum*, 2019, **966**, 451–455, DOI: 10.4028/www.scientific.net/MSF.966.451.
- 16 J. Xiang, Z.-G. Liu, J.-H. Ouyang, Y. Zhou and F.-Y. Yan, Synthesis and electrical conductivity of $\text{La}_{10}\text{Si}_{5.5}\text{B}_{0.5}\text{O}_{27+\delta}$ (B=In, Si, Sn, Nb) ceramics, *Solid State Ionics*, 2012, **220**, 7–11, DOI: 10.1016/j.ssi.2012.05.033.
- 17 D.-Y. Kim and S.-G. Lee, Fabrication and electrical properties of Si-based $\text{La}_{10-x}\text{Bi}_x(\text{SiO}_4)_6\text{O}_3$ apatite ionic conductor, *Mater. Res. Bull.*, 2012, **47**(10), 2856–2858, DOI: 10.1016/j.materresbull.2012.04.056.
- 18 M. Abbassi, R. Ternane, I. Sobrados, A. Madani, M. Trabelsi-Ayadi and J. Sanz, Synthesis, characterization and oxide conduction in Ba doped apatite-type silicates $\text{Ca}_2\text{La}_6\text{Bi}_2(\text{SiO}_4)_6\text{O}_2$, *Mater. Chem. Phys.*, 2014, **147**(1), 285–292, DOI: 10.1016/j.matchemphys.2014.04.041.
- 19 J. R. Tolchard, J. E. H. Sansom, P. R. Slater and M. S. Islam, Effect of Ba and Bi doping on the synthesis and sintering of Ge-based apatite phases, *J. Solid State Electrochem.*, 2004, **8**, 668–673.
- 20 J. E. H. Sansom, D. Richings and P. R. Slater, Powder neutron diffraction study of the oxide-ion-conducting apatite-type phases, $\text{La}_{9.33}\text{Si}_6\text{O}_{26}$ and $\text{La}_8\text{Sr}_2\text{Si}_6\text{O}_{26}$, *Solid State Ionics*, 2001, **139**(3–4), 205–210, DOI: 10.1016/S0167-2738(00)00835-3.
- 21 S. P. Jiang, L. Zhang, H. Q. He, R. K. Yap and Y. Xiang, Synthesis and characterization of lanthanum silicate apatite by gel-casting route as electrolytes for solid oxide fuel cells, *J. Power Sources*, 2009, **189**(2), 972–981, DOI: 10.1016/j.jpowsour.2008.12.064.
- 22 S. Afroze, H. Q. H. H. Absah, M. S. Reza, M. R. Somalu, J.-Y. Park, A. Issakhov and A. K. Azad, Structural and Electrochemical Properties of Lanthanum Silicate Apatites $\text{La}_{10}\text{Si}_{6-x-0.2}\text{Al}_x\text{Zn}_{0.2}\text{O}_{27-\delta}$ for Solid Oxide Fuel Cells (SOFCs), *Int. J. Chem. Eng.*, 2021, DOI: 10.1155/2021/6621373.
- 23 I. Perhaita, L. E. Muresan, A. Nicoara, L. Barbu Tudoran, G. Borodi and L. M. Muresan, Morpho-structural and electrical characterization of Bi-doped apatite-type lanthanum silicates prepared by gel-combustion, *Appl. Phys. A: Mater. Sci. Process.*, 2020, **126**(8), DOI: 10.1007/s00339-020-03818-6.
- 24 T. Yang, H. Zhao, J. Han, N. Xu, Y. Shen, Z. Du and J. Wang, Synthesis and densification of lanthanum silicate apatite electrolyte for intermediate temperature solid oxide fuel cell via co-precipitation method, *J. Eur. Ceram. Soc.*, 2014, **34**(6), 1563–1569.
- 25 S. Afroze, H. Q. H. H. Absah, M. S. Reza, M. R. Somalu, J.-Y. Park, S. Nekoonam, A. Issakhov and A. K. Azad, Structural and Electrochemical Properties of Lanthanum



- Silicate Apatites $\text{La}_{10}\text{Si}_{6-x-0.2}\text{Al}_x\text{Zn}_{0.2}\text{O}_{27-\delta}$ for Solid Oxide Fuel Cells (SOFCs), *Int. J. Chem. Eng.*, 2021, **2021**, 1–10.
- 26 J. Xiang, Z.-G. Liu, J.-H. Ouyang, Y. Zhou and F.-Y. Yan, Synthesis and electrical conductivity of $\text{La}_{10}\text{Si}_{5.5}\text{B}_{0.5}\text{O}_{27+\delta}$ (B = In, Si, Sn, Nb) ceramics, *Solid State Ionics*, 2012, **220**, 7–11.
- 27 Y. T. Malik, A. R. Noviyanti, N. Akbar, I. Hastiawan, T. Saragi and R. Risdiana, Structure, Chemical Stability and Magnetic Properties of Lanthanum Silicate Oxide Apatite Synthesized by Hydrothermal Method, *Mater. Sci. Forum*, 2019, **966**, 415–421.

